Research Article

Periaqueductal gray activates antipredatory neural responses in the amygdala of foraging rats

Eun Joo Kim[1], Mi-Seon Kong[2], Sanggeon Park[4,5], Jeiwon Cho[4,5*], and Jeansok J. Kim[1,3*]

[1]Department of Psychology, University of Washington, Seattle, WA 98195-1525, USA

[2]Department of Psychiatry and Behavioral Sciences, University of Washington, Seattle, WA 98195-1525, USA

[3]Program in Neuroscience, University of Washington, Seattle, WA 98195-1525, USA

[4]Department of Brain and Cognitive Sciences, Scranton College, Ewha Womans University, Seoul, 03760, Republic of Korea

[5]Brain Disease Research Institute, Ewha Brain Institute, Ewha Womans University, Seoul, Republic of Korea

*Jeansok J. Kim, Jeiwon Cho

Email: jeansokk@uw.edu, jelectro21@ewha.ac.kr

Author Contributions:

E.J.K., J.J.K., and J.C. conceived the study. E.J.K. and M.K. performed behavioral, neurophysiological, optogenetic, and tracing experiments. E.J.K., S.G.P., J.C., and J.J.K. analyzed the data. E.J.K., J.C., and J.J.K. wrote the manuscript. J.C. and J.J.K. supervised all aspects of the study.

Keywords:

predator, fear, survival, defensive behavior, decision-making, ethology, single-unit, optogenetics

This PDF file includes:

Main text

Figures 1 to 4

Supplemental Information

Abstract

Pavlovian fear conditioning studies propose that the interaction between the dorsal periaqueductal gray (dPAG) and basolateral amygdala (BLA) functions as a prediction error mechanism for fear memory formation. However, their roles in responding to naturalistic predatory threats, where predictive cues are ambiguous and do not afford reiterative trial-and-error learning, remain unexplored. We conducted single-unit recordings in rats engaged in an ‘approach food-avoid predator’ behavior, characterizing dPAG and BLA neurons responsive to a looming robot predator. Opto-stimulation of dPAG induced fleeing and increased BLA activity. Notably, BLA neurons activated by dPAG stimulation displayed an immediate response to the robot and heightened synchronous activity compared to non-responsive BLA neurons. Furthermore, anterograde and retrograde tracer injections into the dPAG and BLA, respectively, indicate that the paraventricular nucleus of the thalamus (PVT) may mediate dPAG-to-BLA neurotransmission. Our findings suggest that dPAG and BLA interactions, potentially via the PVT, underlie an innate antipredatory defensive mechanism.

Main Text

Introduction

The dPAG and BLA interplay is crucial for defensive mechanisms in animals and humans. For instance, Pavlovian fear conditioning (FC) research, which optimally pairs the conditional stimulus (CS) and unconditional stimulus (US) to elicit conditional fear responses (CRs), suggests that the dPAG functions as part of the ascending pain transmission pathway, providing footshock US information to the BLA, a putative site of CS-US association formation (De Oca et al. 1998, Gross and Canteras 2012, Herry and Johansen 2014, Kim, Rison, and Fanselow 1993, Ressler and Maren 2019, Walker and Davis 1997). Supporting this notion, rodent studies have demonstrated that electrical stimulation of the dPAG, which results in robust bursts of activity (jumping, running, and escaping) akin to footshock-induced unconditional responses (URs) (Jenck, Moreau, and Martin 1995, Olds and Olds 1963), can effectively serve as a surrogate US for both auditory and contextual FC in rats (Di Scala et al. 1987, Kim et al. 2013). In parallel, pharmacological inhibition of PAG has been found to reduce periorbital shock US-elicited behavioral URs and neural responses in the amygdala and impair the acquisition of auditory FC (Johansen et al. 2010). Additionally, it has been shown that while dPAG neurons initially respond to the shock US, the development of fear CRs leads to a decrease in US-evoked neural responses in the PAG due to increased amygdala-PAG pathway-mediated analgesia that dampens the footshock nociception (Johansen et al. 2010). Fundamentally, this negative feedback amygdala-dPAG circuit serves as a biological implementation of the Rescorla–Wagner model (Rescorla and Wagner 1972) of FC (Fanselow 1998). Nonetheless, the significance of PAG-amygdala

interactions observed in small conditioning chambers has yet to be evaluated in more realistic threat scenarios.

In humans undergoing surgery for intractable pain, dPAG stimulation has been observed to provoke intense fear/panic sensations (Carrive and Margan 2012, Magierek et al. 2003). For instance, a patient experiencing PAG stimulation described the sensation as, “Something horrible is coming, somebody is now chasing me, I am trying to escape from him” (Amano et al. 1982). Similarly, we have previously shown that electrical stimulation of either the dPAG or BLA caused naïve rats foraging for food in a naturalistic environment to escape to a safe nest in the absence of external threats (Kim et al. 2013). Moreover, the dPAG stimulation-induced fleeing was dependent on an intact amygdala, whereas the BLA stimulation-induced fleeing was independent of an intact PAG, suggesting that the fear/panic sensations reported in humans are likely due to innate fear information flow from dPAG to BLA. However, it remains unclear how dPAG neurons respond to different predatory threats and how dPAG and BLA communicate threat signals. To address this gap, we employed single-unit recording and optogenetics in our ‘approach food-avoid predator’ paradigm (Choi and Kim 2010, Wang, Chen, and Lin 2015). We characterized dPAG and BLA neurons that were responsive to a looming robot predator and found that dPAG opto-stimulation elicited fleeing and increased BLA activity. Specifically, BLA neurons that were activated by dPAG opto-stimulation demonstrated an immediate response to the robot and exhibited increased synchronous activity in comparison to BLA neurons that were unresponsive to the dPAG opto-stimulation. Additionally, injections of anterograde and retrograde tracers

into the dPAG and BLA, respectively, suggest that the paraventricular nucleus of the thalamus (PVT) may serve as a mediator of dPAG to BLA neurotransmission. These results indicate that dPAG and BLA interactions, possibly via PVT, subserve antipredatory defensive mechanisms.

Results

dPAG neurons respond to extrinsic predatory threats during a risky foraging task

We implanted a microdrive array above the dPAG of five male Long-Evans rats, which were food-restricted to maintain 85% of their normal weight. During baseline sessions, rats were required to procure a food pellet in an open arena (202 cm length x 58 cm width x 6 cm height; Figure 1A) and return to their nest to consume it. The electrodes were gradually lowered (<120 µm/day) into the dPAG during these sessions (Figure 1B). Once well-isolated neural activities were detected, rats underwent predator testing with successive pre-robot, robot, and post-robot sessions (5-15 pellet attempts/session). During the robot session, the animals' outbound foraging time (latency to reach the pellet or the predator-triggering zone) increased, while the pellet success rate decreased (Figures 1C and 1D). We collected a total of 94 dPAG units during predator testing, with 23.4% (n = 22) showing increased firing rates ($z > 3$) specifically to the looming robot with short-latency responses (< 500 ms) during the robot session, but not during the pre- and post-robot sessions (robot cells; Figure 1E and 1F). We focused our analysis on robot cells, excluding other types of units that showed food-specific and mixed robot encounter+pellet procurement responses (pellet and BOTH cells; Figures 1F, S1A, and S1B), to investigate predator-related dPAG

activity. The majority of the robot cells (90.9%) did not show significant correlations between movement speed and neuronal firing rate (Figure S1C). These results suggest that dPAG neurons are involved in detecting a looming robot and eliciting antipredatory defensive behaviors, such as fleeing to a safe nest.

dPAG neurons can intrinsically evoke fear in absence of external threats

We next investigated if optogenetic activation of dPAG neurons could elicit antipredatory behaviors without an external predator. To do so, we first unilaterally injected rats with ChR2 and implanted an optrode into their dPAG (Figures 2A and S2A). In two anesthetized rats, 20-Hz blue light stimulations (437 nm, 10-ms pulse width, 2 s duration) elicited excited responses in 48% of the recorded units (12 out of 25 cells; Figures 2B and S2B), while only one unit showed inhibited responses to the stimulation (Figure S2C), confirming the effectiveness of dPAG opto-stimulation. A separate group of rats with unilateral ChR2 or EYFP injections and optic fiber implantation (Figure 2C) underwent 4 days of baseline training followed by testing sessions. During testing, rats were allowed to procure a pellet without light stimulation (Off) and with light stimulation (On) (Figure 2D). During light-on trials (Figure 2E), the ChR2-expressing animals were not able to procure the pellet and consistently fled into the nest, whether the pellet was placed at a 76.2 cm long distance from the nest (On_L) or at a 25.4 cm short distance from the nest (On_S) (Figures 2F and 2G). However, EYFP control rats did not show any defensive behaviors. Latency to procure pellets increased as a function of the stimulation intensity, frequency, and duration (Figures 2H-2J). These results demonstrate that optical stimulation of CaMKII-expressing dPAG neurons effectively caused naïve

rats approaching a food pellet to flee to the nest without an external threat.

BLA neurons that respond intrinsically to dPAG optical stimulation also respond extrinsically to a robot predator

Our previous data indicated that PAG may transmit innate fear signals to the amygdala (Kim et al. 2013). To investigate amygdala neuron responses to dPAG activity changes, we recorded BLA neurons while optically stimulating the dPAG in foraging rats. Six rats were injected with ChR2 and implanted with an optic fiber in the dPAG and tetrode arrays in the BLA (Figures 3A). After the electrodes were lowered to the target structures between the baseline sessions, animals underwent testing comprising of pre-stim, stim, and post-stim sessions (Figure 3B). The dPAG stimulation increased outbound foraging time (Figure 3C) and decreased success rate (Figure 3D), mimicking predator-induced cautious behavior (Figures 1C and 1D). While rats were escaping the foraging area without the pellet (stim session), we collected data from 322 BLA neurons. Subsets of neurons in the BLA (n=32) exhibited immediate firing increases in response to dPAG stimulation (Figures 3E and S3A-C).

To further investigate how stimulation-responsive neurons respond to an actual predator, three out of the six rats were tested with a looming robot following the post-stim session (Figure 3F). The predatory robot increased outbound foraging time compared to the post-stim session (Figure 3G). Among the 85 units recorded in the BLA, robot-specific cells increased firing in response to the looming robot (robot cells; BLA, 25.9%; Figures S3D-F). Correlation analysis revealed that 95.4% of BLA robot cells did not show significant correlations between firing rates and movement speed (Figure S3G). Additionally, 23/85 BLA units were responsive to optical stimulation

during the stim session but not pre/post-stim sessions (Figures 3H and 3I). The proportions of the robot and non-robot cells differed between stimulation-responsive and nonresponsive cells, with a lower proportion of robot cells in the stimulation-nonresponsive cells (Figures 3J). Stimulation-responsive cells exhibited higher firing rates to the robot predator than stimulation-nonresponsive cells (Figures 3K, S3H, and S3I). The higher the maximal firing rate was during the stimulation, the greater the cells fired to the actual robot predator (Figures 3L).

We computed cross-correlations between simultaneously recorded BLA cell pairs to test how subpopulations of BLA neurons co-activate to the predatory threat differently. From 66 BLA recorded neurons, 185 BLA pairs were computed for cross-correlograms (CCs) during post-robot surge (2-s periods subsequent to robot activation; robot session), post-pellet, and post-stim (2-s periods subsequent to pellet procurement; pre- and post-stim sessions) epochs. Twenty-six CCs showed significant peaks (z scores > 3) around the paired spikes (between 0 ms to 100 ms) during the post-surge epoch (Figure S4A). Cell pairs with spike synchrony during the post-robot surge epoch did not show correlated firing during the post-pellet or post-stim epochs (Figures 3M, S4B, and S4C). This effect was prominent when pairs contained at least one of the stimulation-responsive cells (stim pairs; Figures 3N, S4D, and S4E), but not when pairs include only stimulation-nonresponsive cells (non-stim pairs; Figures 3N, S4D, and S4F). Stim pairs exhibited greater synchronous firing compared to non-stim pairs during the 0-50 ms window but had lower correlated firing during the 50-100 ms window, indicating that dPAG-stimulation responsive cells fire together more closely than dPAG-stimulation non-

responsive cells (Figures 3O and S4G). Additionally, the stim pairs tended to have higher peaks of the cross-correlograms than the non-stim pairs (Figure S4H). Taken together, these results suggest that dPAG stimulation produces activity changes in subpopulations of BLA neurons, primarily in predator detection cells (robot cells), supporting the idea that PAG conveys innate fear signals to the amygdala.

The PVT interconnects the dPAG and BLA

Based on previous anatomical studies (Cameron et al. 1995, Krout and Loewy 2000) and response latency data in the present study (Figures S3B and S3C), it is likely that projections from the dPAG to the BLA are indirect. To identify potential mediators that relay predator signals from the dPAG to the BLA, we injected the anterograde tracer AAV-CaMKII-EYFP into the dPAG and investigated robot-induced c-Fos activities in AAV-expressed terminal areas of the dPAG. Cholera toxin subunit B (CTB) was injected into the BLA in a subset of AAV-injected animals (n = 6) to examine potential anatomical evidence of relays between the dPAG and BLA (Figures 4A and 4B). After recovery, rats were trained to procure a pellet from the foraging arena. Animals were randomly assigned to foraging-only and robot-experienced groups. The foraging-only group quickly procured the pellet, while the robot-experienced group failed during the testing session (Figure 4C). Ninety minutes after testing, animals were perfused to analyze the tracers and c-Fos activity. We found strong terminal expression in midline thalamic areas emerging from dPAG cell body infection (Figure 4D). Among these, the paraventricular nucleus of the thalamus (PVT) showed increased levels of c-Fos-positive cells in rats encountering the robot predator compared to controls (Figures 4E and 4F). Subpopulations of the PVT c-Fos-positive cells also expressed CTB injected in

the BLA (Figures 4G and 4H), suggesting predator-induced dPAG activity transmits information to the BLA, possibly through PVT activity.

Discussion

Prehistoric rock carvings and cave drawings of large carnivores from the Ice Age suggest that the fear of predation played a crucial role in the lives of early humans in their habitats (Mithen 1999). As such, the brain's fear system, which evolved to counteract unpredictable, uncontrolled threats originating from biological agents, likely influences our everyday behavior when confronted with perceived risks. In line with this view, studies using functional magnetic resonance imaging (fMRI) and an 'active escape paradigm'—in which virtually represented subjects are chased by a virtual predator and receive an electric shock when "caught"—have shown that as the threat transitions from a distant position to an impending encounter with the subject, neural activity shifts from the ventromedial PFC and amygdala towards the PAG (Mobbs et al. 2009, Mobbs et al. 2007).

The present study investigated the neural mechanisms underlying antipredatory defensive behaviors in rats engaged in a naturalistic goal-directed behavior of foraging for food in an open arena, using a combination of electrophysiology, optogenetics, and tracing techniques. We found that neurons in the dPAG are involved in detecting predatory threats and eliciting antipredatory defensive behaviors in rats. Specifically, dPAG neurons displayed increased spiking in response to a looming robot predator as rats reflexively fled from the open foraging arena into a safe nest. However, dPAG neuronal activity did not increase when the

robot was stationary, which contrasts with a previous study that reported enhanced dPAG neuronal activity in mice exposed to an anesthetized (motionless) rat separated by a wire mesh in a chamber (Deng, Xiao, and Wang 2016) or a live rat tethered (restrainted) with a harness (Reis et al. 2021). It has been suggested that looming stimuli may serve as simple, evolutionarily-reliable signals of danger because genes are not capable of providing the brain with detailed information about all potential predatory threats, and all predators must approach their prey for consumption (Kim and Jung 2018). Our study also demonstrated that optogenetic stimulation of CaMKII-expressing dPAG neurons caused naïve rats approaching a food pellet to instantly flee to the nest without an external threat (see also (Tsang et al. 2023)). This confirmed that the original report of escape behavior in foraging rats with electrical stimulation of dPAG (Kim et al. 2013) was indeed evoked by intrinsic dPAG neurons and not the fibers of passage or spreading of currents to other brain regions. In contrast to our observation of escape-to-the-nest behavior, optogenetic activation of dPAG in mice elicited various defensive behaviors, such as running, freezing and conditioned avoidance, when tested in a chamber (Deng, Xiao, and Wang 2016). This is consistent with the notion that the behavioral outcome from brain stimulation is influenced by environmental settings (Kim et al. 2013).

Our study also revealed that BLA neurons respond both intrinsically to dPAG optical stimulation and extrinsically to a robot predator. Specifically, BLA cells that were responsive to dPAG stimulation showed increased firing rates and tended to be co-activated in response to the predatory threat more than dPAG stimulation-non-responsive BLA cells. Moreover, BLA firings in response to dPAG stimulation was highly

correlated with their firings in response to the actual predatory agent. These findings, combined with earlier studies demonstrating that the amygdala is necessary for both intrinsic dPAG stimulation-induced (Kim et al. 2013) and extrinsic robot-evoked (Choi and Kim 2010) escape behavior, suggests that the dPAG-amygdala pathway is involved in processing innate fear signals and generating antipredatory defensive behavior.

Lastly, we confirmed strong terminal expressions in the midline thalamic areas (Cameron et al. 1995, Krout and Loewy 2000) following AAV injection into the dPAG using immunohistochemistry. We also observed that the PVT, but not other midline thalamic subregions, showed increased c-Fos reactivity to the robot predator, consistent with a recent study showing dPAG projections to the PVT, not the centromedial intralaminar thalamic nucleus (Yeh, Ozawa, and Johansen 2021). Subpopulations of the c-Fos-reactive PVT neurons were also found to express CTB, which was retrogradely labeled by injection into the BLA. This study's findings, combined with previous reports on the involvement of the dPAG, PVT, and BLA in producing flight behaviors in naïve rats (Choi and Kim 2010, Daviu et al. 2020, Deng, Xiao, and Wang 2016, Kim et al. 2013, Kim et al. 2018, Kong et al. 2021, Ma et al. 2021, Reis et al. 2021), suggest that the dPAG→PVT→BLA pathways play a critical role in antipredatory defensive mechanisms in rats (Figure 4I) (Reis et al. 2023). Given the results from other research groups that emphasize the importance of the superior colliculus in detecting innate visual threats (Lischinsky and Lin 2019, Wei et al. 2015, Zhou et al. 2019), it is important to further investigate whether the activity of the superior colliculus changes in response to external predatory threats

and to elucidate how the superior colliculus and the dPAG-BLA circuitry communicate.

The innate predator-fear functions of the dPAG and BLA are distinct from their learned fear functions, as observed in FC studies. In FC, the dPAG is proposed to play a role in “US-processing,” transmitting footshock (pain) information to the amygdala, thus enhancing the CS pathway’s ability to activate the amygdalar fear system (Fanselow 1998, Maren 2001, Almeida, Roizenblatt, and Tufik 2004). This hypothesis is supported by research demonstrating that muscimol inactivation of the dPAG hinders FC to the footshock US (Johansen et al. 2010), while electrical stimulation of dPAG neurons effectively serves as a US surrogate for FC (Ballesteros et al. 2014, Kim et al. 2013). As conditioning progresses, amygdalar fear may suppress footshock-evoked dPAG’s teaching signals, thereby moderating FC in the amygdala, potentially through conditioned analgesia that dampens the footshock US’s painfulness (Fanselow 1981, Fanselow and Bolles 1979). Consistent with this amygdalar-dPAG negative feedback notion, research has revealed that as CS-evoked responses of amygdalar neurons increase with CS-US pairings, footshock-evoked neural activity in the dPAG decreases (Johansen et al. 2010, Ozawa et al. 2017, Quirk, Repa, and LeDoux 1995). It remains to be determined whether there are distinct populations of innate predator-responsive and pain-responsive dPAG neurons or if the same dPAG neurons react to a wide range of aversive stimuli. Furthermore, it is worth noting that the same dPAG stimulation resulted in an activity burst UR in a small operant chamber, as opposed to a goal-directed escape to a nest UR in a large foraging arena (Kim et al. 2013). Additionally, FC to shock or predator US does not readily occur in naturalistic settings (Zambetti et al. 2022).

Overall, this study enhances our understanding of the neural basis of antipredatory defensive behaviors in rats, emphasizing the important roles of the dPAG and BLA in processing and responding to threat-related stimuli. The study also suggests the possibility of an innate fear mechanism, which may complement the commonly studied learned fear mechanism in the research of anxiety and fear-related disorders. Further research into these mechanisms could lead to the development of novel therapeutic interventions that target both innate and learned fear mechanisms, improving the treatment of anxiety and fear-related disorders.

Materials and Methods

Subjects

Male and female Long-Evans rats (initial weight 325-350 g) were individually housed in a climate-controlled vivarium (accredited by the Association for Assessment and Accreditation of Laboratory Animal Care), with a reversed 12-h light/dark cycle (lights on at 7 PM) and placed on a standard food-restriction schedule with free access to water to gradually reach ~85% normal body weights. All experiments were performed during the dark cycle in compliance with the University of Washington Institutional Animal Care and Use Committee guidelines.

Surgery

Under anesthesia (94 mg/kg ketamine and 6 mg/kg xylazine, intraperitoneally), rats were mounted in a stereotaxic instrument (Kopf) and implanted with a Microdrive of tetrode bundles (formvar-insulated nichrome wires, 14 µm diameter; Kanthal) into the dPAG (AP, -6.8; ML, +0.6; from Bregma), or BLA (AP, -2.8; ML, +5.2; from Bregma).

For optogenetic stimulation, anesthetized male rats were injected with Adeno-associated viruses (AAVs; serotype 5) to express Channelrhodopsin-EYFP (AAV5-CaMKIIa-hChR2(H134R)-EYFP, UNC Vector Core) or EYFP only (AAV5-CaMKIIa-EYFP) in the dPAG at a rate of 0.05 µl/min (total volume of 0.5 µl) via a microinjection pump (UMP3-1, World Precision Instruments) with a 33-gauge syringe (Hamilton). To avoid backflow of the virus, the injection needle was left in place for 10 min. After virus injection, an optic fiber attached to ferrules (0.22 NA, 200 µm core; ferrule diameter: 2.5 mm; Doric Lenses) or an optrode was implanted 0.4 mm dorsal to the injection sites. The microdrive and/or ferrule were secured by Metabond and dental cement with anchoring screws. Behavioral and recording experiments started after at least one week of recovery while optogenetic stimulation sessions started after at least 4 weeks after the surgery to allow for sufficient viral expression. For tracing experiments, male and female rats were injected with AAV-CamKII-EYFP into the dPAG and CTB into the BLA three months and one week prior to the predator testing, respectively.

Foraging apparatus

A custom-built foraging arena comprised a nest (29 cm x 57 cm x 60 cm height) and a foraging area (202 cm length x 58 cm width x 6 cm height) with a V-shaped gate connecting the two areas. The animals' movement was automatically tracked via two video tracking systems (Neuralynx and Any-maze).

Behavioral procedures

(Habituation) Animals were placed in the nest area, where they were acclimated to the experimental room and chamber and allowed to eat food pellets (0.5 g; F0171, Bio-Serv) for 30 min/day for 2 consecutive days.

(Baseline foraging) After the animals were placed in the nest, the gate to the foraging area opened, and the animals explored the arena and were gradually trained to acquire a food pellet from various locations (25 cm, 50 cm, and 75 from the nest for the behavior-only experiment; additional 100 cm and 125 cm distance trials for the recording experiment). Once the rat procured the pellet and returned to the nest, the gate closed. The behavior-only groups underwent 4 days of baseline foraging training. For the recording experiments, baseline sessions were continued until dPAG or amygdala unit activity was successfully detected.

(Testing) For dPAG recordings, single units were recorded throughout three successive pre-robot, robot, and robot sessions (5-15 trials/session). During the pre- and post-robot trials, the rat was allowed to freely procure the pellet. Before the robot trials started, the programmed robot (LEGO Mindstorms EV3 set) was placed at the end of the foraging arena. Once the gate opened, every time the rat came near (~25 cm) the pellet, the programmed robot surged 23, 60, or 140 cm toward the animal at a velocity of 20-52 cm/s and then returned backward to the original position. If the rat made another attempt within 10 s after the previous robot activation, both the previous and following trials were not included in the analyses to exclusively measure the unit properties. For optical stimulation and behavioral experiments, the testing consisted of 3 baseline trials with a 75 cm pellet location and 3 dPAG stimulation trials with sequential 75 cm, 50 cm, and 25 cm pellet locations. Each time the rat approached the pellet, 473-nm light stimulation (1-2 s, 20-Hz, 10-ms width, 0.25-3 mW) was given to the rat through a laser (Opto Engine LLC) and a pulse generator (Master-8; A.M.P.I.). If the rat failed to procure the pellet within 3 min, the gate closed, and the trial ended. For amygdala

recording with optical stimulation of dPAG, pre-stim, stim, and post-stim sessions were conducted. The three consecutive procedures were the same with the pre-robot, robot, and post-robot sessions, except that the dPAG light stimulation was given instead of the robot predator. A subset of the animals (n = 3) additionally underwent the robot session following the post-stim session.

Optrode recording under anesthesia

Upon optrode implantation, the animal was kept under anesthesia and moved to a unit recording setup (Neuralynx). The electrode was slowly lowered, and dPAG activity was monitored. Once dPAG activity was detected, eight light stimulations (2 s, 20-Hz, 10-ms width) were given with 30-s inter-stimulus intervals. Ten and fourteen stimulation sessions were repeated in the two anesthetized rats, respectively. After the recording was completed, the animal was immediately perfused under an overdose of Beuthanasia. Only the unit data collected in the dPAG were included in the analyses after histological verification.

Single-unit recording and analyses

Extracellular single unit activity was recorded through a 24-channel microdrive array loaded with a bundle of six tetrodes. The electrode tip was gold-plated to 100-300 kΩ measured at 1 kHz. The signals were amplified (×10,000), filtered (600-6000 kHz), and digitized (32 kHz) using a Cheetah data acquisition system (Neuralynx). A spike-sorting program (SpikeSort 3D; Neuralynx) and additional manual cutting were used for cluster isolation. Peri-event time histograms (PETH) were generated using NeuroExplorer (version 5.030; Nex Technologies) and further analyzed with custom MATLAB programs. The unit and speed data were binned at 0.1 s or 1 s and aligned to the time

when the robot was activated, when the pellet was procured, or when the rat turned its body immediately before fleeing to the nest. All PETH data were normalized (*z*-scored) to the pre-stimulus baseline period (-5 s to 0 s to the pellet procurement or robot activation). To classify the responsiveness of the unit responses, the first five bins (0.1-s bins) were analyzed. If one or more bins within the 500-ms period showed *z*-scores higher than 3 ($z > 3$) exclusively during the robot session, then the unit was classified as a 'robot cell'. The rest of the cells were further classified as food-specific ($z > 3$ exclusively during pre-robot session), BOTH ($z > 3$ during both pre-robot and robot sessions), or none (non-responsive) cells. In the light stimulation and recording experiments, the same criteria were applied to the unit classification except that the stimulation-responsive units (stim cells) were defined as cells showing significant activity ($z > 3$) during the stim session when aligned to the stimulation onset instead of the robot activation.

Cross-correlation

BLA cells that were simultaneously recorded from rats undergoing the four successive sessions (pre-stim, stim, post-stim, and robot sessions) were analyzed to generate cross-correlograms (CCs). Units firing less than 0.1 Hz were excluded due to the possible false peaks in their CCs. The shift predictors (100 random trial shuffles) were subtracted from the raw CCs. The correlated firing (in 10-ms bins) during the 0-2 s period following robot activation was calculated, and the CCs that showed significant peaks ($z > 3$) within the 0-100 ms window during the robot session were further analyzed. The peak values of the CCs and the peak areas under CC curves during the 100-ms window were compared across sessions (pre-stim, stim, post-stim, and robot

sessions).

Histology

To verify the electrode placement, rats were overdosed with Beuthanasia, given electrolytic currents (10 µA, 10 s) in the target regions through the tetrode tips, and perfused intracardially with 0.9% saline and then 10% formalin. For rats injected with the virus, phosphate-buffered saline (PBS) and 4% paraformaldehyde were used as perfusates. Extracted brains were stored in the fixative at 4 °C overnight followed by 30% sucrose solution until they sank. Transverse sections (50 µm) were mounted on gelatin-coated slides and stained with cresyl violet and Prussian blue dyes to examine the recording sites. To confirm viral expression, 30-µm sections were cut, mounted, and cover-slipped with Flouromount-GTM with DAPI (eBioscience). Immunohistochemistry was performed on some of the sections to visualize the viral and c-Fos expressions. In short, the sections were washed with 0.1M phosphate buffered saline (PBS) for 10 min three times, followed by three rinses with PBS with Triton X-100 (PBST). After two hours of blocking (using normal goat serum), the sections were incubated in primary antibodies (1:500 mouse anti-GFP and rabbit anti-c-Fos; Abcam) overnight. The following day, additional PBST washes and secondary antibodies (1:500 anti-mouse Alexa 488 and anti-rabbit Alexa 405; Abcam) were applied. The sections were examined under a fluorescence microscope (Keyence BZ-X800E) and analyzed using ImageJ (NIH). Only rats with correct viral expression or electrode/optic fiber tip locations in the target structure(s) were included for the statistical analyses (Figure S5).

Statistical analyses

Based on normality tests (Kolmogorov-Smirnov test, $P < 0.01$), non-normally

distributed variables were analyzed using non-parametric tests, while parametric tests were applied to normally distributed variables. Statistical significance across sessions was determined using the Friedman test, followed by Dunn's multiple comparison test with correction when needed. Pearson's correlation coefficients evaluated variable relationships, and Chi-square tests compared percentages of distinct unit types. Group comparisons involved independent *t*-tests or Mann-Whitney U tests, and within-group comparisons employed paired *t*-tests or Wilcoxon signed rank tests. Statistical analyses and graph generation were performed using SPSS (ver. 19), custom MATLAB codes, GraphPad Prism (ver. 9.00), and NeuroExplorer (ver. 5.030).

Data availability

The data that support the findings of this study and the relevant analysis code will be available from the Dryad data repository upon the acceptance of the article.

Acknowledgments

This study was supported by the National Institutes of Health grants MH099073 (J.J.K.), AG067008 (E.J.K.), and F32MH127801 (M.K.), and the Ministry of Science and ICT through the National Research Foundation of Korea grant: Brain Science Research Program NRF-2022M3E5E8018421 (J.C.) and NRF-2022R1A2C2009265 (J.C.). Cartoons in Figures 1E, 2D, 3B, and 3F were created with BioRender.com.

Disclosures

All authors report no biomedical financial interests or potential conflicts of interests.

References

Almeida, T. F., S. Roizenblatt, and S. Tufik. 2004. "Afferent pain pathways: a neuroanatomical review." *Brain Res* 1000 (1-2):40-56. doi: 10.1016/j.brainres.2003.10.073.

Amano, K., T. Tanikawa, H. Kawamura, H. Iseki, M. Notani, H. Kawabatake, T. Shiwaku, T. Suda, H. Demura, and K. Kitamura. 1982. "Endorphins and pain relief. Further observations on electrical stimulation of the lateral part of the periaqueductal gray matter during rostral mesencephalic reticulotomy for pain relief." *Appl Neurophysiol* 45 (1-2):123-35.

Ballesteros, C. I., B. de Oliveira Galvao, S. Maisonette, and J. Landeira-Fernandez. 2014. "Effect of dorsal and ventral hippocampal lesions on contextual fear conditioning and unconditioned defensive behavior induced by electrical stimulation of the dorsal periaqueductal gray." *PLoS One* 9 (1):e83342. doi: 10.1371/journal.pone.0083342.

Cameron, A. A., I. A. Khan, K. N. Westlund, and W. D. Willis. 1995. "The efferent projections of the periaqueductal gray in the rat: a Phaseolus vulgaris-leucoagglutinin study. II. Descending projections." *J Comp Neurol* 351 (4):585-601. doi: 10.1002/cne.903510408.

Carrive, P, and M. M. Margan. 2012. "Periaqueductal Gray." In *The Human Nervous System*, edited by J. K.; Paxinos Mai, G., 367-400. London: Academic Press.

Choi, J. S., and J. J. Kim. 2010. "Amygdala regulates risk of predation in rats foraging in a dynamic fear environment." *Proc Natl Acad Sci U S A* 107 (50):21773-7. doi: 10.1073/pnas.1010079108.

Daviu, N., T. Fuzesi, D. G. Rosenegger, N. P. Rasiah, T. L. Sterley, G. Peringod, and J. S. Bains. 2020. "Paraventricular nucleus CRH neurons encode stress controllability and regulate defensive behavior selection." *Nat Neurosci* 23 (3):398-410. doi: 10.1038/s41593-020-0591-0.

De Oca, B. M., J. P. DeCola, S. Maren, and M. S. Fanselow. 1998. "Distinct regions of the periaqueductal gray are involved in the acquisition and expression of defensive responses." *J Neurosci* 18 (9):3426-32. doi: 10.1523/JNEUROSCI.18-09-03426.1998.

Deng, H., X. Xiao, and Z. Wang. 2016. "Periaqueductal Gray Neuronal Activities Underlie Different Aspects of Defensive Behaviors." *J Neurosci* 36 (29):7580-8. doi: 10.1523/JNEUROSCI.4425-15.2016.

Di Scala, G., M. J. Mana, W. J. Jacobs, and A. G. Phillips. 1987. "Evidence of Pavlovian conditioned fear following electrical stimulation of the periaqueductal grey in the rat." *Physiol Behav* 40 (1):55-63. doi: 10.1016/0031-9384(87)90185-5.

Fanselow, M. S. 1981. "Naloxone and Pavlovian fear conditioning." *Learning and Motivation* 12 (4):398-419.

Fanselow, M. S. 1998. "Pavlovian conditioning, negative feedback, and blocking: mechanisms that regulate association formation." *Neuron* 20 (4):625-7. doi: 10.1016/s0896-6273(00)81002-8.

Fanselow, M. S., and R. C. Bolles. 1979. "Triggering of the endorphin analgesic reaction by a cue previously associated with shock: Reversal by naloxone. ." *Bulletin of the Psychonomic Society* 14:88-90.

Furigo, I. C., W. F. de Oliveira, A. R. de Oliveira, E. Comoli, M. V. Baldo, S. R. Mota-Ortiz, and N. S. Canteras. 2010. "The role of the superior colliculus in predatory hunting." *Neuroscience* 165 (1):1-15. doi: 10.1016/j.neuroscience.2009.10.004.

Gross, C. T., and N. S. Canteras. 2012. "The many paths to fear." *Nat Rev Neurosci* 13 (9):651-8. doi: 10.1038/nrn3301.

Herry, C., and J. P. Johansen. 2014. "Encoding of fear learning and memory in distributed neuronal circuits." *Nat Neurosci* 17 (12):1644-54. doi: 10.1038/nn.3869.

Jenck, F., J. L. Moreau, and J. R. Martin. 1995. "Dorsal periaqueductal gray-induced aversion as a simulation of panic anxiety: elements of face and predictive validity." *Psychiatry Res* 57 (2):181-91. doi: 10.1016/0165-1781(95)02673-k.

Johansen, J. P., J. W. Tarpley, J. E. LeDoux, and H. T. Blair. 2010. "Neural substrates for expectation-modulated fear learning in the amygdala and periaqueductal gray." *Nat Neurosci* 13 (8):979-86. doi: 10.1038/nn.2594.

Kim, E. J., O. Horovitz, B. A. Pellman, L. M. Tan, Q. Li, G. Richter-Levin, and J. J. Kim. 2013. "Dorsal periaqueductal gray-amygdala pathway conveys both innate and learned fear responses in rats." *Proc Natl Acad Sci U S A* 110 (36):14795-800. doi: 10.1073/pnas.1310845110.

Kim, E. J., M. S. Kong, S. G. Park, S. J. Y. Mizumori, J. Cho, and J. J. Kim. 2018. "Dynamic coding of predatory information between the prelimbic cortex and lateral amygdala in foraging rats." *Sci Adv* 4 (4):eaar7328. doi: 10.1126/sciadv.aar7328.

Kim, J. J., and M. W. Jung. 2018. "Fear paradigms: The times they are a-changin'." *Curr Opin Behav Sci* 24:38-43. doi: 10.1016/j.cobeha.2018.02.007.

Kim, J. J., R. A. Rison, and M. S. Fanselow. 1993. "Effects of amygdala, hippocampus, and periaqueductal gray lesions on short- and long-term contextual fear." *Behav Neurosci* 107 (6):1093-8. doi: 10.1037//0735-7044.107.6.1093.

Kong, M. S., E. J. Kim, S. Park, L. S. Zweifel, Y. Huh, J. Cho, and J. J. Kim. 2021. "'Fearful-place' coding in the amygdala-hippocampal network." *Elife* 10. doi: 10.7554/eLife.72040.

Krout, K. E., and A. D. Loewy. 2000. "Periaqueductal gray matter projections to midline and intralaminar thalamic nuclei of the rat." *J Comp Neurol* 424 (1):111-41. doi: 10.1002/1096-9861(20000814)424:1<111::aid-cne9>3.0.co;2-3.

Kunwar, P. S., M. Zelikowsky, R. Remedios, H. Cai, M. Yilmaz, M. Meister, and D. J. Anderson. 2015. "Ventromedial hypothalamic neurons control a defensive emotion state." *Elife* 4. doi: 10.7554/eLife.06633.

Li, Z., J. X. Wei, G. W. Zhang, J. J. Huang, B. Zingg, X. Wang, H. W. Tao, and L. I. Zhang. 2021. "Corticostriatal control of defense behavior in mice induced by auditory looming cues." *Nat Commun* 12 (1):1040. doi: 10.1038/s41467-021-21248-7.

Lischinsky, J. E., and D. Lin. 2019. "Looming Danger: Unraveling the Circuitry for Predator Threats." *Trends Neurosci* 42 (12):841-842. doi: 10.1016/j.tins.2019.10.004.

Ma, J., J. du Hoffmann, M. Kindel, B. S. Beas, Y. Chudasama, and M. A. Penzo. 2021. "Divergent projections of the paraventricular nucleus of the thalamus mediate the selection of passive and active defensive behaviors." *Nat Neurosci* 24 (10):1429-1440. doi: 10.1038/s41593-021-00912-7.

Magierek, V., P. L. Ramos, N. G. da Silveira-Filho, R. L. Nogueira, and J. Landeira-Fernandez. 2003. "Context fear conditioning inhibits panic-like behavior elicited by electrical stimulation of dorsal periaqueductal gray." *Neuroreport* 14 (12):1641-4.

doi: 10.1097/00001756-200308260-00020.
Maren, S. 2001. "Neurobiology of Pavlovian fear conditioning." *Annu Rev Neurosci* 24:897-931. doi: 10.1146/annurev.neuro.24.1.897.
Menegas, W., K. Akiti, R. Amo, N. Uchida, and M. Watabe-Uchida. 2018. "Dopamine neurons projecting to the posterior striatum reinforce avoidance of threatening stimuli." *Nat Neurosci* 21 (10):1421-1430. doi: 10.1038/s41593-018-0222-1.
Mithen, S. 1999. *The Prehistory of the Mind: The Cognitive Origins of Art, Religion and Science.* London: Thames & Hudson.
Mobbs, D., J. L. Marchant, D. Hassabis, B. Seymour, G. Tan, M. Gray, P. Petrovic, R. J. Dolan, and C. D. Frith. 2009. "From threat to fear: the neural organization of defensive fear systems in humans." *J Neurosci* 29 (39):12236-43. doi: 10.1523/JNEUROSCI.2378-09.2009.
Mobbs, D., P. Petrovic, J. L. Marchant, D. Hassabis, N. Weiskopf, B. Seymour, R. J. Dolan, and C. D. Frith. 2007. "When fear is near: threat imminence elicits prefrontal-periaqueductal gray shifts in humans." *Science* 317 (5841):1079-83. doi: 10.1126/science.1144298.
Olds, M. E., and J. Olds. 1963. "Approach-avoidance analysis of rat diencephalon." *J Comp Neurol* 120:259-95. doi: 10.1002/cne.901200206.
Ozawa, T., E. A. Ycu, A. Kumar, L. F. Yeh, T. Ahmed, J. Koivumaa, and J. P. Johansen. 2017. "A feedback neural circuit for calibrating aversive memory strength." *Nat Neurosci* 20 (1):90-97. doi: 10.1038/nn.4439.
Quirk, G. J., C. Repa, and J. E. LeDoux. 1995. "Fear conditioning enhances short-latency auditory responses of lateral amygdala neurons: parallel recordings in the freely behaving rat." *Neuron* 15 (5):1029-39. doi: 10.1016/0896-6273(95)90092-6.
Reis, F. M., J. Y. Lee, S. Maesta-Pereira, P. J. Schuette, M. Chakerian, J. Liu, M. Q. La-Vu, B. C. Tobias, J. M. Ikebara, A. H. Kihara, N. S. Canteras, J. C. Kao, and A. Adhikari. 2021. "Dorsal periaqueductal gray ensembles represent approach and avoidance states." *Elife* 10. doi: 10.7554/eLife.64934.
Reis, Fmcv, D. Mobbs, N. S. Canteras, and A. Adhikari. 2023. "Orchestration of innate and conditioned defensive actions by the periaqueductal gray." *Neuropharmacology* 228:109458. doi: 10.1016/j.neuropharm.2023.109458.
Rescorla, R. A., and A. R. Wagner. 1972. "A theory of Pavlovian conditioning: Variations in the effectiveness of reinforcement and nonreinforcement." In *Classical conditioning II: Current research and theory*, edited by A. H. Black and W. F. Prokosy, 64–99. New York: Appleton-Century-Crofts.
Ressler, R. L., and S. Maren. 2019. "Synaptic encoding of fear memories in the amygdala." *Curr Opin Neurobiol* 54:54-59. doi: 10.1016/j.conb.2018.08.012.
Rhoades, R. W., R. D. Mooney, W. H. Rohrer, M. M. Nikoletseas, and S. E. Fish. 1989. "Organization of the projection from the superficial to the deep layers of the hamster's superior colliculus as demonstrated by the anterograde transport of Phaseolus vulgaris leucoagglutinin." *J Comp Neurol* 283 (1):54-70. doi: 10.1002/cne.902830106.
Silva, B. A., C. Mattucci, P. Krzywkowski, E. Murana, A. Illarionova, V. Grinevich, N. S. Canteras, D. Ragozzino, and C. T. Gross. 2013. "Independent hypothalamic circuits for social and predator fear." *Nat Neurosci* 16 (12):1731-3. doi: 10.1038/nn.3573.

Tsang, E., C. Orlandini, R. Sureka, A. H. Crevenna, E. Perlas, I. Prankerd, M. E. Masferrer, and C. T. Gross. 2023. "Induction of flight via midbrain projections to the cuneiform nucleus." *PLoS One* 18 (2):e0281464. doi: 10.1371/journal.pone.0281464.

Walker, D. L., and M. Davis. 1997. "Involvement of the dorsal periaqueductal gray in the loss of fear-potentiated startle accompanying high footshock training." *Behav Neurosci* 111 (4):692-702. doi: 10.1037//0735-7044.111.4.692.

Wang, L., I. Z. Chen, and D. Lin. 2015. "Collateral pathways from the ventromedial hypothalamus mediate defensive behaviors." *Neuron* 85 (6):1344-58. doi: 10.1016/j.neuron.2014.12.025.

Wei, P., N. Liu, Z. Zhang, X. Liu, Y. Tang, X. He, B. Wu, Z. Zhou, Y. Liu, J. Li, Y. Zhang, X. Zhou, L. Xu, L. Chen, G. Bi, X. Hu, F. Xu, and L. Wang. 2015. "Processing of visually evoked innate fear by a non-canonical thalamic pathway." *Nat Commun* 6:6756. doi: 10.1038/ncomms7756.

Yeh, L. F., T. Ozawa, and J. P. Johansen. 2021. "Functional organization of the midbrain periaqueductal gray for regulating aversive memory formation." *Mol Brain* 14 (1):136. doi: 10.1186/s13041-021-00844-0.

Zambetti, P. R., B. P. Schuessler, B. E. Lecamp, A. Shin, E. J. Kim, and J. J. Kim. 2022. "Ecological analysis of Pavlovian fear conditioning in rats." *Commun Biol* 5 (1):830. doi: 10.1038/s42003-022-03802-1.

Zhou, Z., X. Liu, S. Chen, Z. Zhang, Y. Liu, Q. Montardy, Y. Tang, P. Wei, N. Liu, L. Li, R. Song, J. Lai, X. He, C. Chen, G. Bi, G. Feng, F. Xu, and L. Wang. 2019. "A VTA GABAergic Neural Circuit Mediates Visually Evoked Innate Defensive Responses." *Neuron* 103 (3):473-488 e6. doi: 10.1016/j.neuron.2019.05.027.

Figures

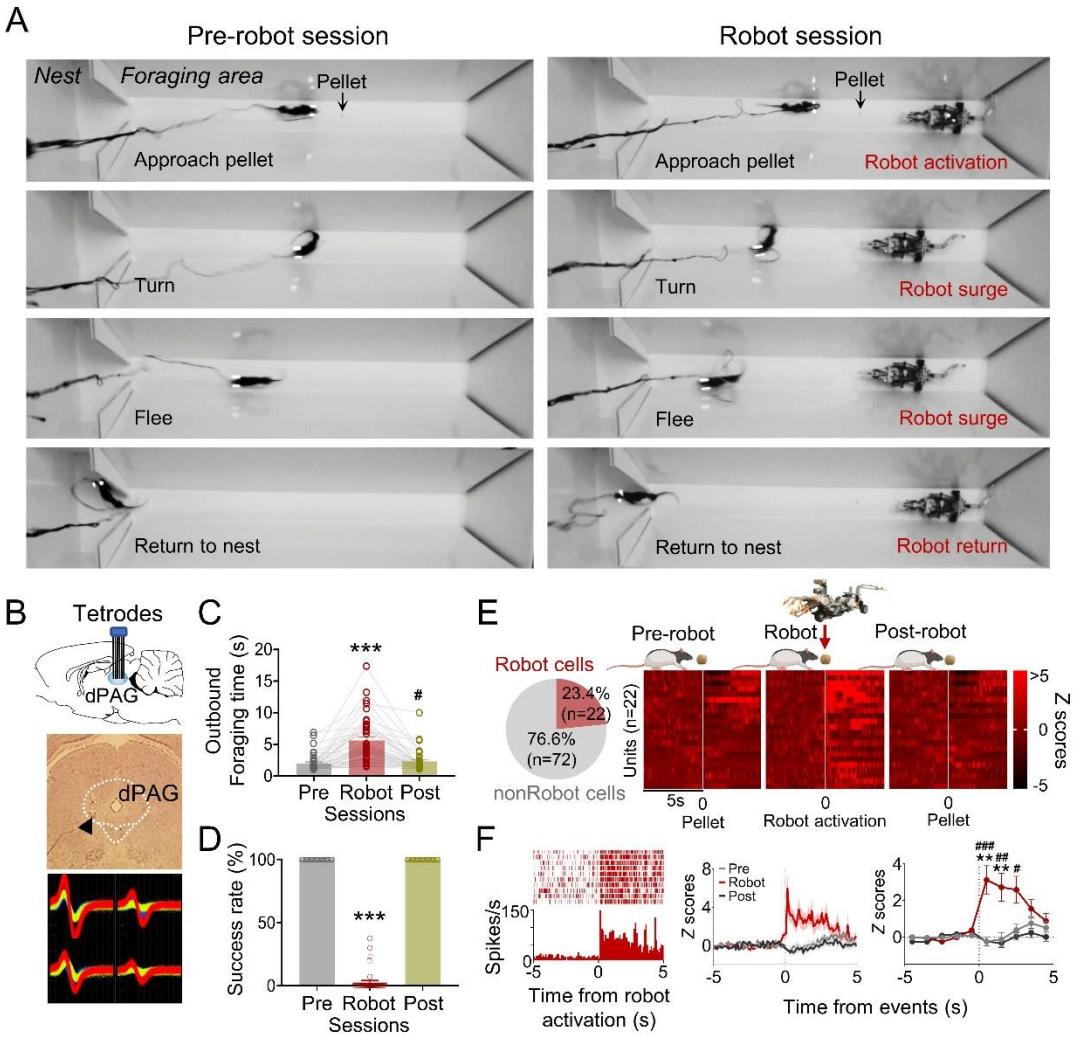

Figure 1. dPAG single unit recordings during risky foraging. (A) Rats underwent pre-robot, robot, and post-robot sessions, successfully securing pellets in pre- and post-robot trials, and failing during robot trials due to robot surge. (B) Tetrode implantation in dPAG with photomicrographs of the tip (arrowhead) and unit clusters/waveforms. (C) Outbound foraging time increased during the robot session (X^2 = 64.00, P < 0.0001, Friedman test; *P*s < 0.05 for all comparisons, Dunn's test). ****P* < 0.001 compared to pre-robot and post-robot sessions. #*P* < 0.05 compared to the pre-robot session. (D)

Pellet success rate decreased during robot session (X^2 = 84.00, P < 0.0001, Friedman test; Ps < 0.0001 for all comparisons, Dunn's test). ***P < 0.001 compared to pre-robot and post-robot sessions. (E) Cell type proportions showed 23.4% cells responding to robot activation (robot cells). (F) Representative dPAG robot cell raster/event histogram aligned with robot activations, and population activity of robot cells around robot activation time (t = 0) with 0.1 s and 1 s bins. Firing rates of the robot cells were higher during robot session (0-3 s blocks; Friedman test, all X^2s > 6.952, all Ps < 0.05; Dunn's test, all Ps < 0.05). Shaded areas indicate SEM. **P < 0.01 compared to pre-robot session. #, ##, and ### denote P < 0.05, P < 0.01, and P < 0.001 respectively, compared to post-robot session.

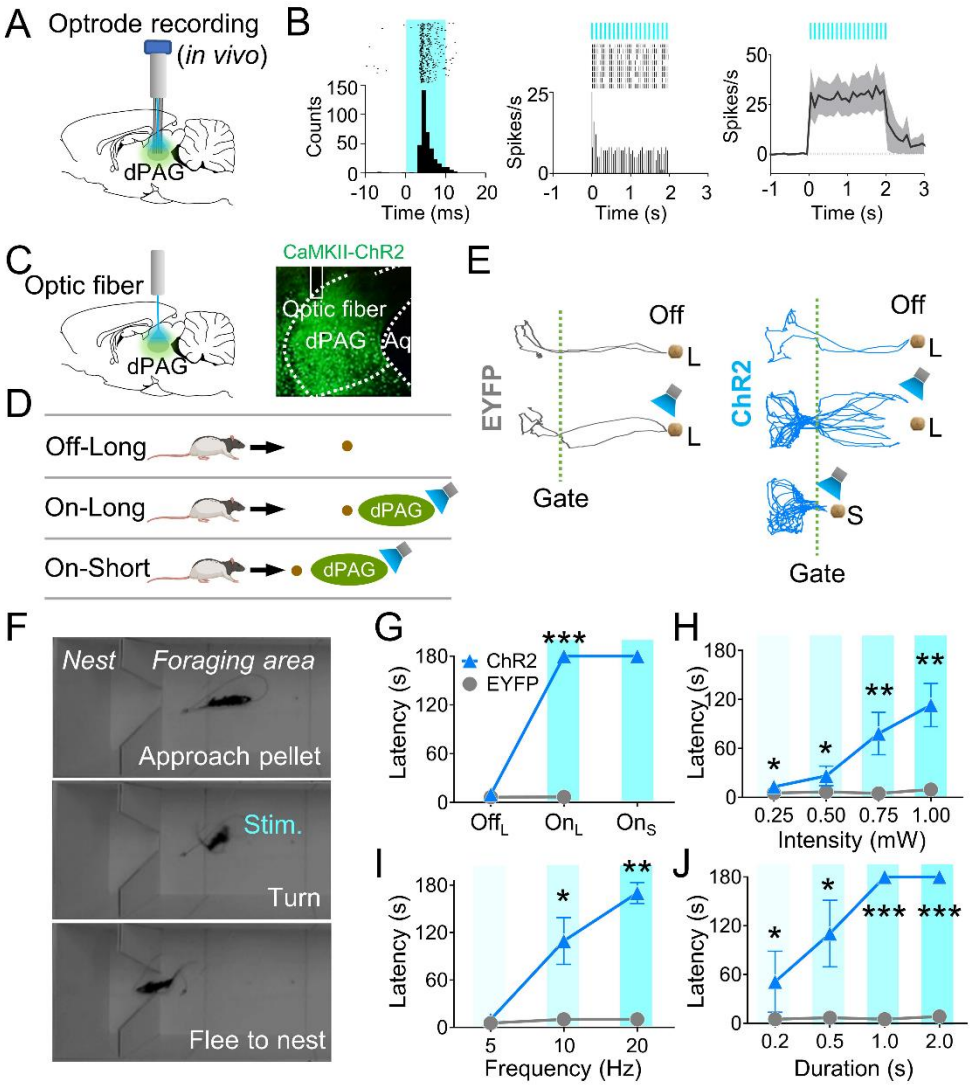

Figure 2. dPAG optical stimulation evokes fear. (A) Virus injection, optrode implantation in dPAG, and light stimulation during single unit recordings in anesthetized rats. (B) Raster plots and peri-event time histograms for 20-Hz light stimulations (10-ms width, *left*; 2-s duration, *center*). 48% of 25 units had increased firing during 2-s light stimulation (*right*). (C) Virus injection, expression, and optic fiber placement in dPAG. (D) Stimulation testing: baseline trials at 75-cm distance (Long) without light; stimulation trials with 2-s light as the rat approached (~25 cm) Long pellet; light applied as the rat

approached 25-cm (Short) pellet if Long pellet unsuccessful. (E) Representative trajectories for EYFP- and ChR2-expressing rats during stimulation testing. (F) Rat behaviors during light stimulation trials. (G) ChR2 rats showed increased latency to procure pellet upon opto-stimulation (On_L) compared to EYFP rats (Off_L, $Z = 1.013$, $P = 0.311$; On_L, $U = 0.0$, $P < 0.001$; Mann-Whitney U test). (H-J) ChR2 group exhibited increased latency to procure pellet compared to EYFP group based on stimulation intensity (H; *U*s < for all intensities < 3.5, *P*s for all intensities < 0.025; Mann-Whitney U test), frequency (I; *U*s for 10 Hz and 20 Hz < 2.5, *P*s for 10 and 20 Hz < 0.014; Mann-Whitney U test), and duration (J; *U*s for all durations < 4.5, *P*s for all durations < 0.032; Mann-Whitney U test). *, **, and *** denote $P < 0.05$, $P < 0.01$, and $P < 0.001$, respectively.

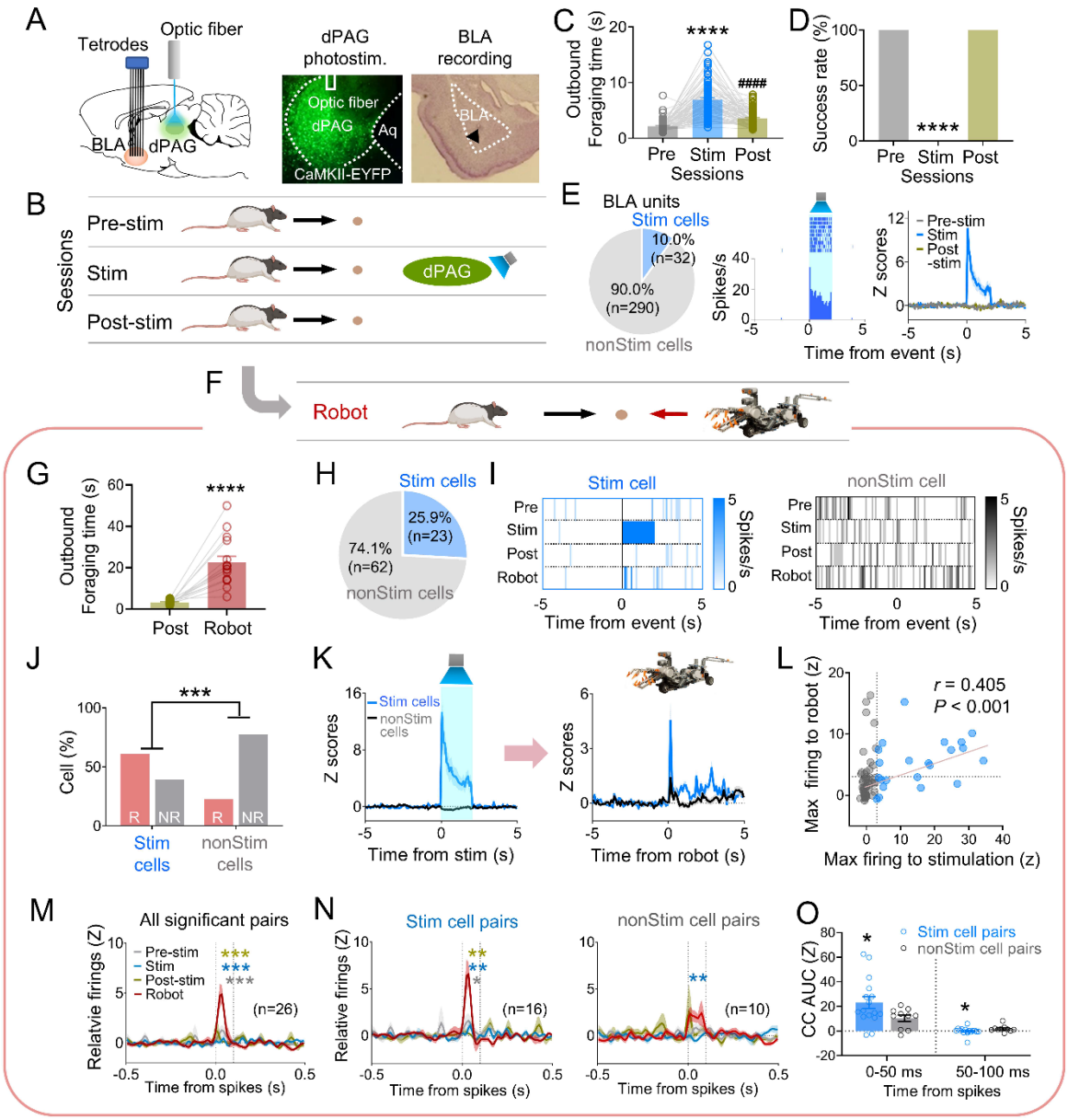

Figure 3. dPAG optical stimulation and amygdala single-unit recordings. (A) Virus injection in dPAG and tetrode array implantation targeting BLA. Light stimulation during single-unit recordings in freely-moving rats. (B) Stimulation testing sessions: in pre- and post-stim trials, rats freely procured pellets; in stim trials, optical stimulation prevented procurement of pellets. (C,D) During dPAG stimulation, animals showed increased

outbound foraging time (C; X^2 = 117.8, P < 0.0001, Friedman test; Ps < 0.0001, Dunn's test) and decreased success rate (D; X^2 = 154.0, P < 0.0001, Friedman test; Ps < 0.0001, Dunn's test). ****P < 0.0001 compared to pre-robot and post-robot sessions. ####P < 0.0001 compared pre-robot session. (E) Subset of BLA units (10.0%) responsive to optical stimulation (Stim cells; *left*), and a representative (*center*) and all stimulation-responsive (nonStim cells; *right*) raster plots with PETHs. (F) Subset of animals underwent additional robot trials following the post-stim session. (G) Increased outbound foraging time during robot session compared to post-stimulation session (t(15) = 6.655, P < 0.0001; paired t-test). ****P < 0.0001. (H) Twenty-two BLA units were dPAG stimulation-responsive. (I) Representative raster plots of dPAG stimulation-responsive and -nonresponsive units. (J) Proportions of robot vs. non-robot cells differed between stimulation-responsive and -nonresponsive units (X^2 = 11.134, P < 0.001; Chi-squared test). ***P < 0.001. (K) PETHs of stim and non-stim cells during stimulation and robot sessions. (L) Relationship between maximal firing rates during first 500 ms subsequent to robot activation and maximal firing rates during first 500 ms after stimulation onset (r(85) = 0.405, P < 0.001; Pearson correlation). (M) Population CCs with significant synchrony during robot session were higher than other sessions. Dotted vertical lines indicate 0-100 ms window for testing significance. Grey, blue, and dark yellow ***P < 0.001 compared to pre-stimulation, stimulation, and post-stimulation sessions, respectively. (N) Among synchronized BLA cell pairs, those including dPAG stimulation-responsive cell(s) (stim pairs; 61.5%) showed increased correlated firings (area under the curve, AUC, during 0-100 ms window) during the robot session compared to other sessions. In contrast, synchronized BLA cell pairs that consisted of

stimulation non-responsive cells only showed no AUC differences across sessions. Grey *, blue **, and dark yellow ***P* < 0.05 compared to pre-stimulation, *P* < 0.01 compared to stimulation, and *P* < 0.001 compared to post-stimulation sessions, respectively. (O) Comparing CCs during testing windows (0-50 ms and 50-100 ms) between stim and non-stim pairs, stim pairs exhibited higher correlated firing than non-stim pairs during the 0-50 ms block ($t(21.99) = 2.342$, $P = 0.0286$; *t*-test), while displaying decreased correlated firings in the second block (50-100 ms; $U = 42$, $P = 0.045$; Mann-Whitney U test). **P* < 0.05 compared to the non-stim pairs.

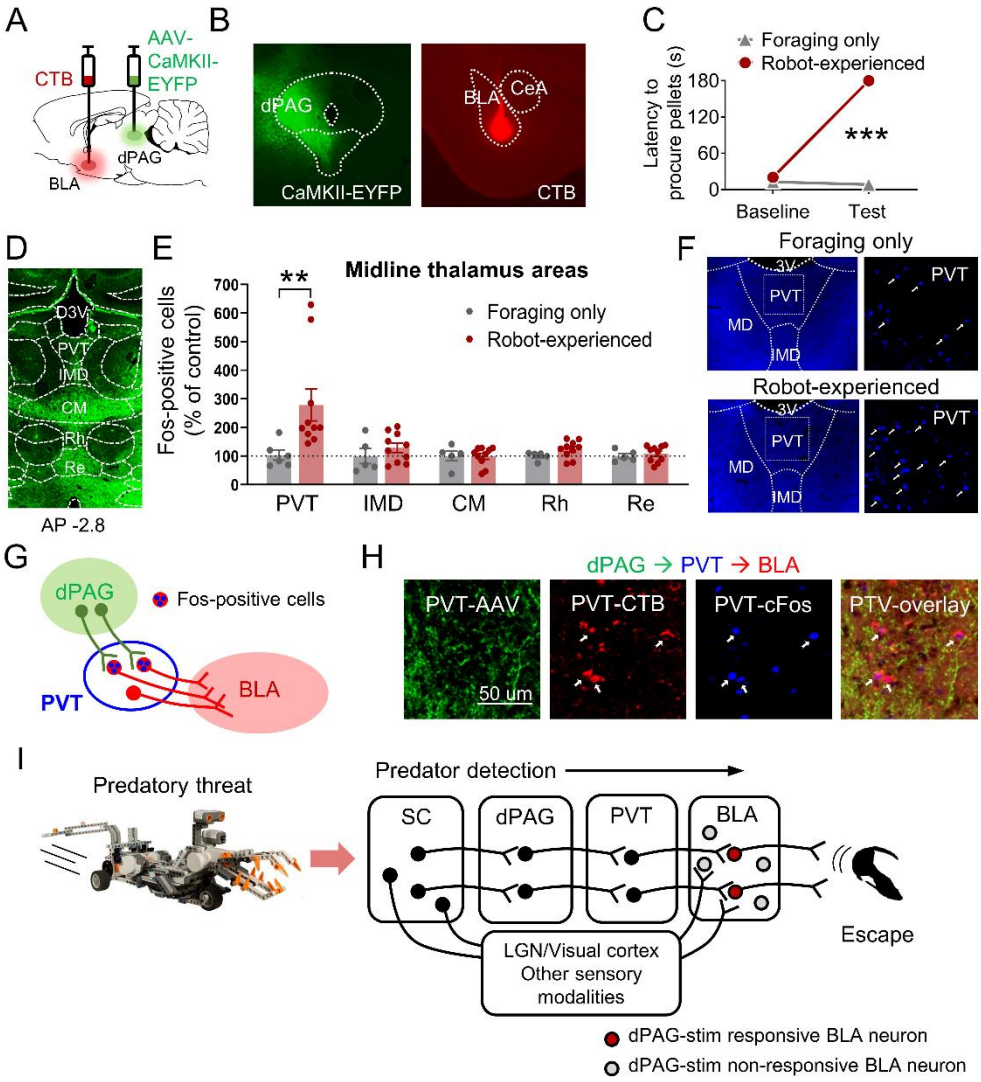

Figure 4. PVT as a potential mediator of dPAG signals to amygdala and a hypothesized model of the dPAG-amygdala circuit in anti-predatory behaviors. (A) Retrograde tracer CTB injected into the BLA and AAV-CaMKII-EYFP injected into the dPAG to explore candidate areas conveying dPAG signals to the BLA. (B) Representative images of AAV and CTB expressions in dPAG and BLA, respectively. (C) Rats encountering the robot predator failed to procure pellets, while foraging-only animals succeeded (Base, $U = 26$, $P = 0.6926$; Test, $U = 0$, $P = 0.0001$; Mann-Whitney

U test). ***$P < 0.001$ compared to the foraging-only group. (D) Terminal expressions of AAV injected into the dPAG cell bodies were predominantly observed in the midline nuclei of the thalamus. (E) PVT showed higher c-Fos-positive cells in robot-experienced rats compared to foraging-only control rats ($U = 3.0$, $P = 0.0016$; Mann-Whitney U test), while other midline thalamic areas showed no differences (Us > 12.0, Ps > 0.129; Mann-Whitney U test). **$P < 0.01$ compared to the foraging-only group. (F) Representative photomicrographs of PVT c-Fos staining from foraging-only (upper) and robot-experienced (bottom) rats. (G) Schematic of triple staining in the PVT. (H) Triple staining of AAV, CTB, and c-Fos in the PVT suggests it might mediate predator information from the dPAG to the BLA. (I) A putative predatory fear circuit model: Predator surge detected by visual pathways, such as the superior colliculus (Furigo et al. 2010, Rhoades et al. 1989), is transmitted to the dPAG, then to the PVT, which excites the BLA. The BLA projects to regions involved in executing escape responses, such as the ventral striatum (Li et al. 2021, Menegas et al. 2018) and ventromedial hypothalamus (Silva et al. 2013, Kunwar et al. 2015, Wang, Chen, and Lin 2015).

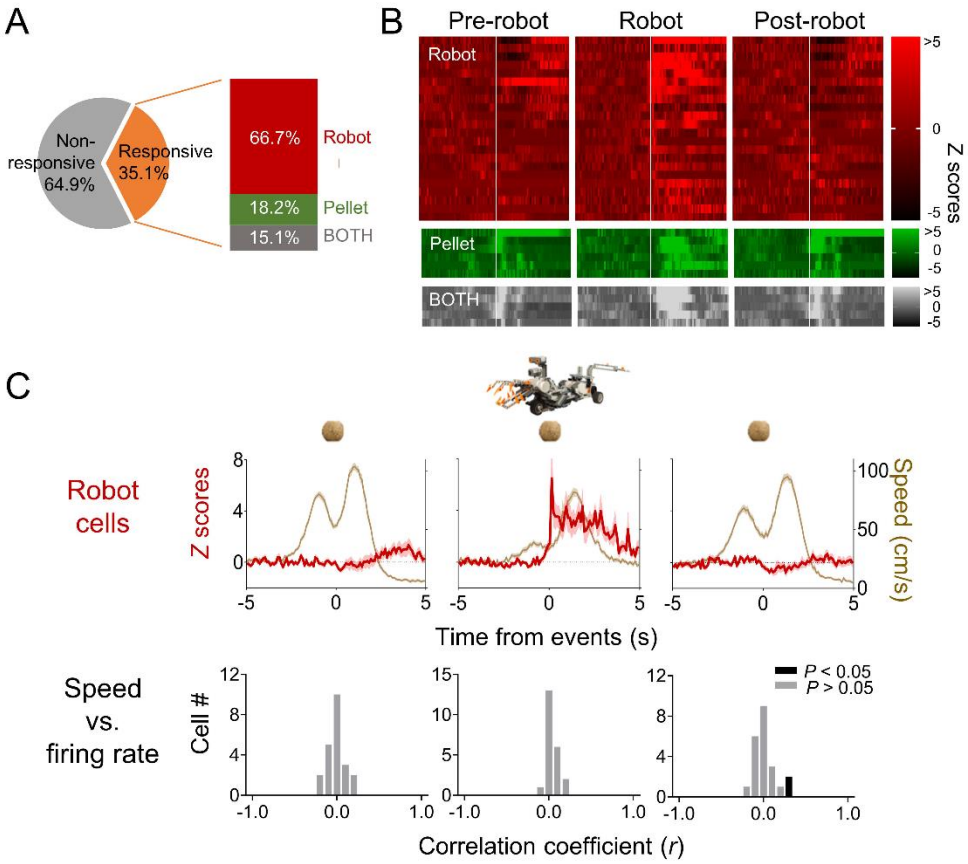

Figure S1. Cell types of the dPAG units. (A) A subset (35.1%) of dPAG neurons increased firing rates in response to the robot, food pellet, or both. Among them, 66.7% of dPAG neurons responded exclusively to the robot. Units were classified as “robot cells” if their z-score was greater than 3 in one or more bins during the robot phase and less than 3 during the pre-robot phase. Conversely, units were classified as “pellet cells" if their z-score was greater than 3 during the pre-robot phase and less than 3 during the robot phase. If the z-score was greater than 3 in both the pre-robot and robot phases, those units were classified as “BOTH cells.” (B) Raster plots showing all robot, pellet, and BOTH cells during pre-robot, robot, and post-robot sessions. (C-E) The top row in each group of cells shows the mean firing rate and movement speed (± SEM; shaded

areas) during the pre-robot, robot, and post-robot sessions. The bottom rows show the correlation coefficients between the firing rate and movement speed during each session in the robot (C), pellet (D), and BOTH (E) cell groups.

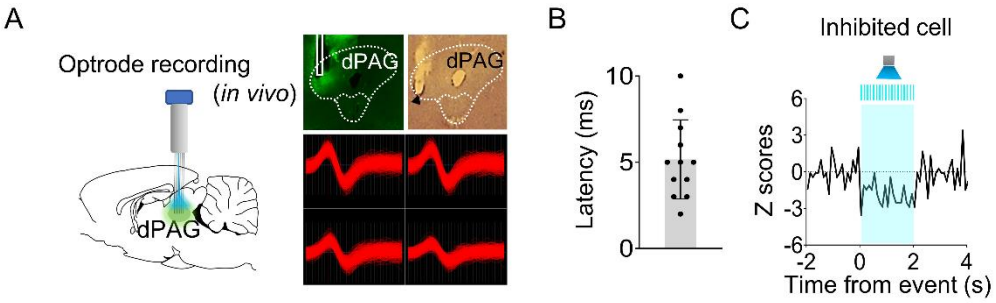

Figure S2. Optrode recording of the dPAG. (A) Virus was injected in the dPAG and an optrode was implanted targeting the dPAG (*left*). Photomicrographs show virus expression and optic fiber/electrode tips, as well as a representative dPAG neuron (*right*). Light stimulation was delivered while single units were recorded in anesthetized rats. (B) Response latencies of the stimulation-responsive dPAG cells. (C) There was one dPAG cell showing inhibited responses to the optical stimulation of the dPAG.

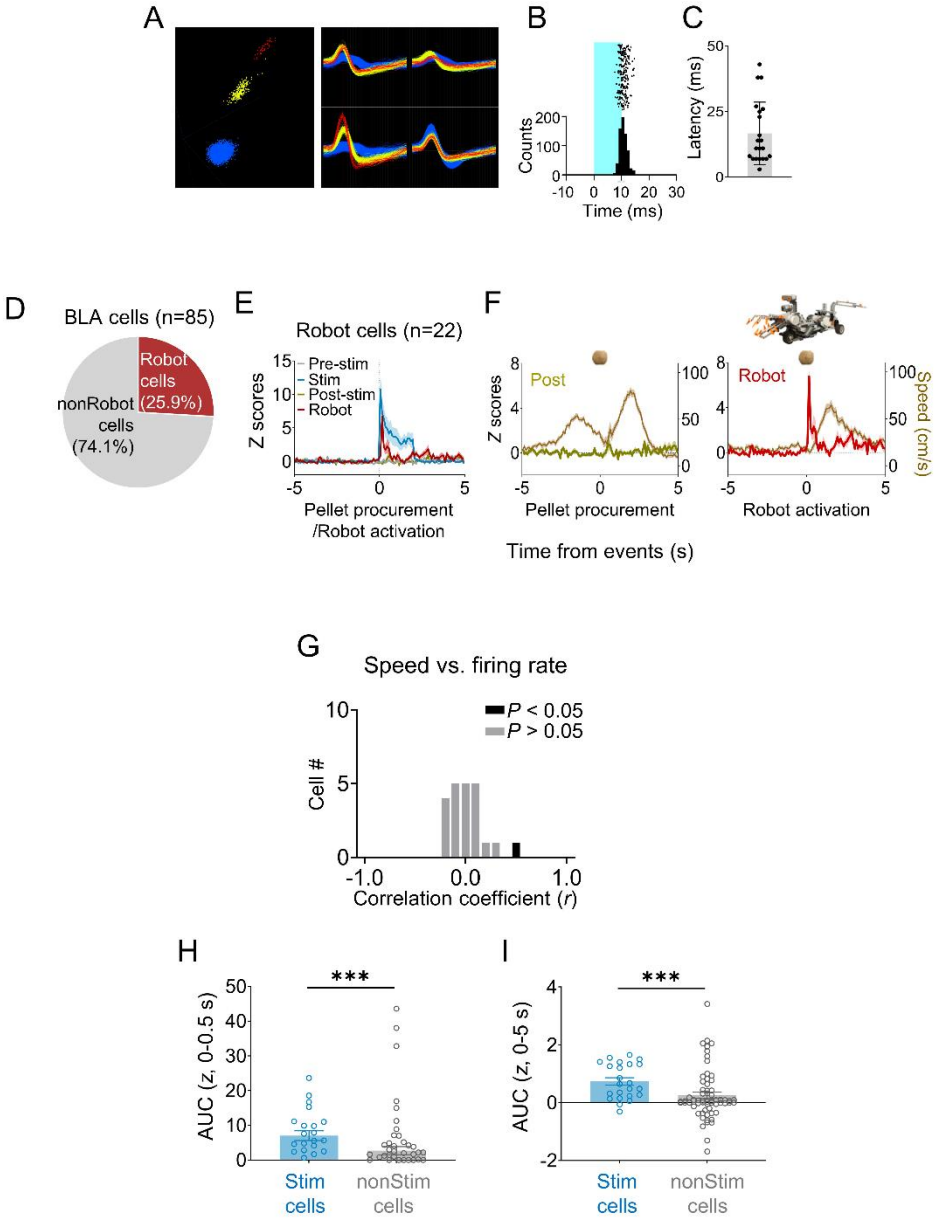

Figure S3. Characteristics of BLA cells. (A) Among 85 units collected from the BLA, 25.9% units immediately responded to the robot. (B) Representative waveforms of the BLA cells. (C) A representative raster plot and peri-event time histograms to the 20-Hz light stimulations (10-ms pulse width, 2-s duration). (D) Response latencies of the BLA cells that responded to the dPAG stimulation. (E) A pre-event time histogram showing the BLA activity aligned to the pellet procurement (pre-stim and post-stim sessions),

dPAG stimulation (stim session), or robot activation (robot session). (F) The firing rates of the robot cells and movement speeds were plotted for the pellet procurement (post-robot session) and the robot activation (robot sessions). (G) All BLA cells, except for one, showed no significant correlation between the firing rate and the movement speed. (H, I) dPAG stimulation-responsive units showed higher levels of robot-evoked firings compared to the stimulation-non-responsive units during the short (H; 0-0.5 s after robot activation; $U = 339.0$, $P = 0.0001$; Mann-Whitney U test) and long-lasting (I; 0-5 s after robot activation; $U = 384.5$, $P = 0.0009$; Mann-Whitney U test) time windows. *** denotes $P < 0.001$ compared to the non-stim pairs.

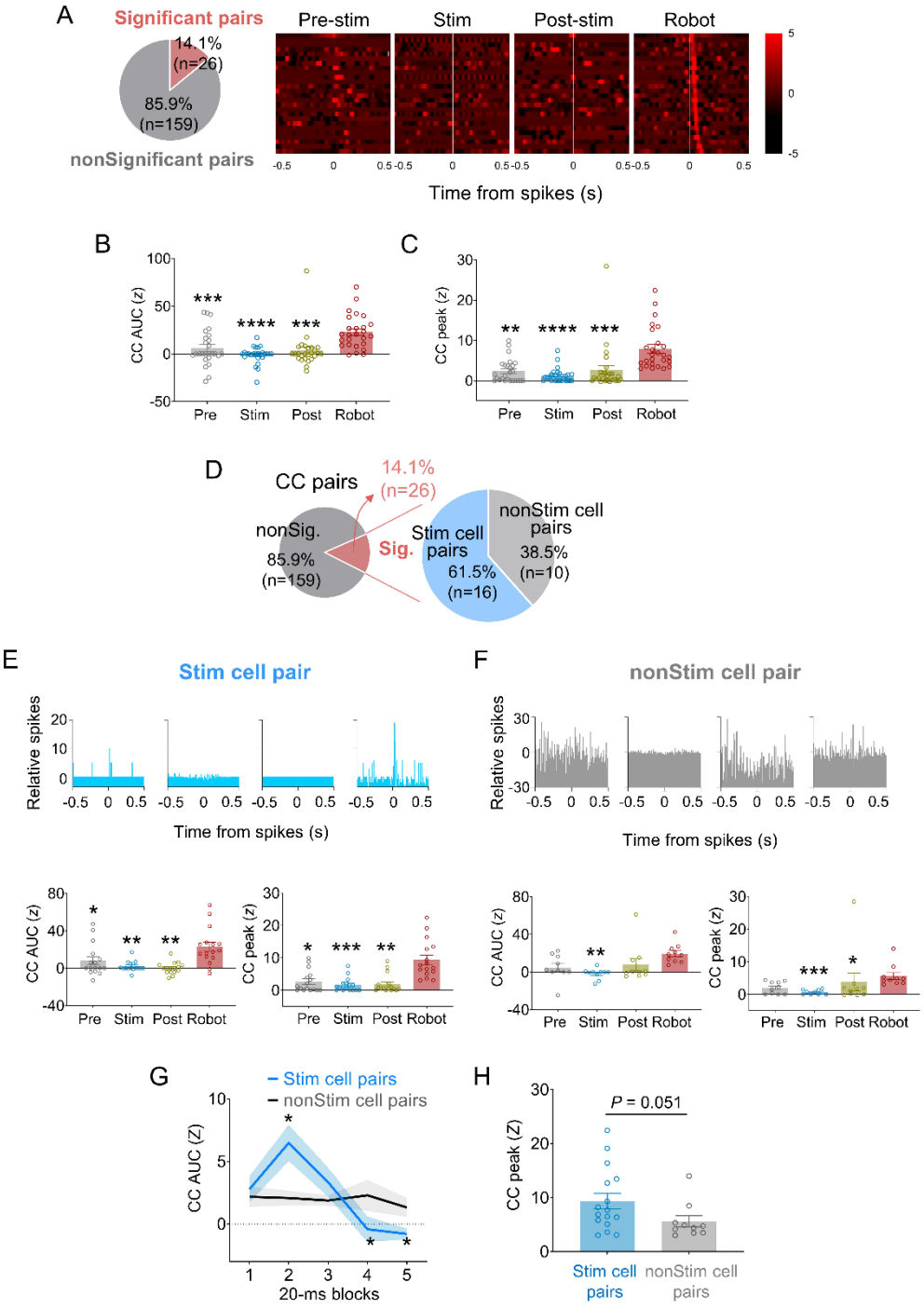

Figure S4. Spike synchrony of the dPAG stimulation-responsive BLA neurons under predatory threats. (A) Among the 185 CCs of the simultaneously recorded BLA neurons, 14.1% of the pairs showed significant ($z > 3$) peaks during the robot session.

(B, C) The mean CC AUCs (B) and CC peak values (C) were higher during the robot session compared to the other sessions (Zs > 29.36, P < 0.0001, Friedman test; Ps < 0.01 for pre-stimulation vs. robot, stimulation vs. robot, and post-stimulation vs. robot sessions comparisons, Dunn's test). **, ***, and **** denote P < 0.01, P < 0.001, and P < 0.0001 compared to the robot session, respectively. (D) Among the BLA cell pairs that significantly synchronized during the robot session, 61.5% of the pairs (stim pairs) included dPAG stimulation-responsive BLA cells while 38.5 % of the pairs (non-stim pairs) did not. (E) Spike synchrony of the stim pairs. A representative CC of a stim pair (*top*) showed increased correlated firing during the robot session. The mean CC AUC (*bottom, left*) and CC peak (*bottom right*) of stim pairs during the robot session were higher than those during the other sessions (Zs > 17.42, P < 0.001, Friedman test; Ps < 0.037 for pre-stimulation vs. robot, stimulation vs. robot, and post-stimulation vs. robot sessions comparisons, Dunn's test). *, **, and *** denote P < 0.05, P < 0.01, and P < 0.001 compared to the robot session, respectively. (F) Spike synchrony of the non-stim pairs. The representative CCs show significant correlated firing during the robot session in the non-stim pairs (*top*). The CC AUC (*bottom left*) did not differ between the robot and pellet-only sessions (pre- and post-stim sessions) while peak area during the robot session was higher than that during the stim session (Z = 13.84, P < 0.01, Friedman test; P = 0.0017 for the stimulation vs. robot sessions comparison, Dunn's test). The CC peak (*bottom right*) during the robot session was higher than those during the stimulation and post-stimulation sessions (Z = 15.92, P < 0.01, Friedman test; Ps < 0.0335 for stimulation vs. robot and post-stimulation vs. robot sessions comparisons, Dunn's test), but not the pre-stimulation session. *, **, and *** denote P < 0.05, P <

0.01, and $P < 0.001$ compared to the robot session, respectively. (G) Stim pairs showed higher correlated firings than the non-stim pairs during the 20-40 ms time period after the paired cell fired ($U = 32$, $P = 0.011$; Mann-Whitney U test) while they showed lower correlated firings than the non-stim pairs during the 60-100 ms time window of the CCs (60-100 ms; Us < 37, Ps < 0.023; Mann-Whitney U test). * denotes $P < 0.05$ compared to the non-stim pairs. (H) The CC peaks of the stim pairs during the robot session tended to be higher than those of the non-stim pairs ($U = 43.0$, $P = 0.051$; Mann-Whitney U test).

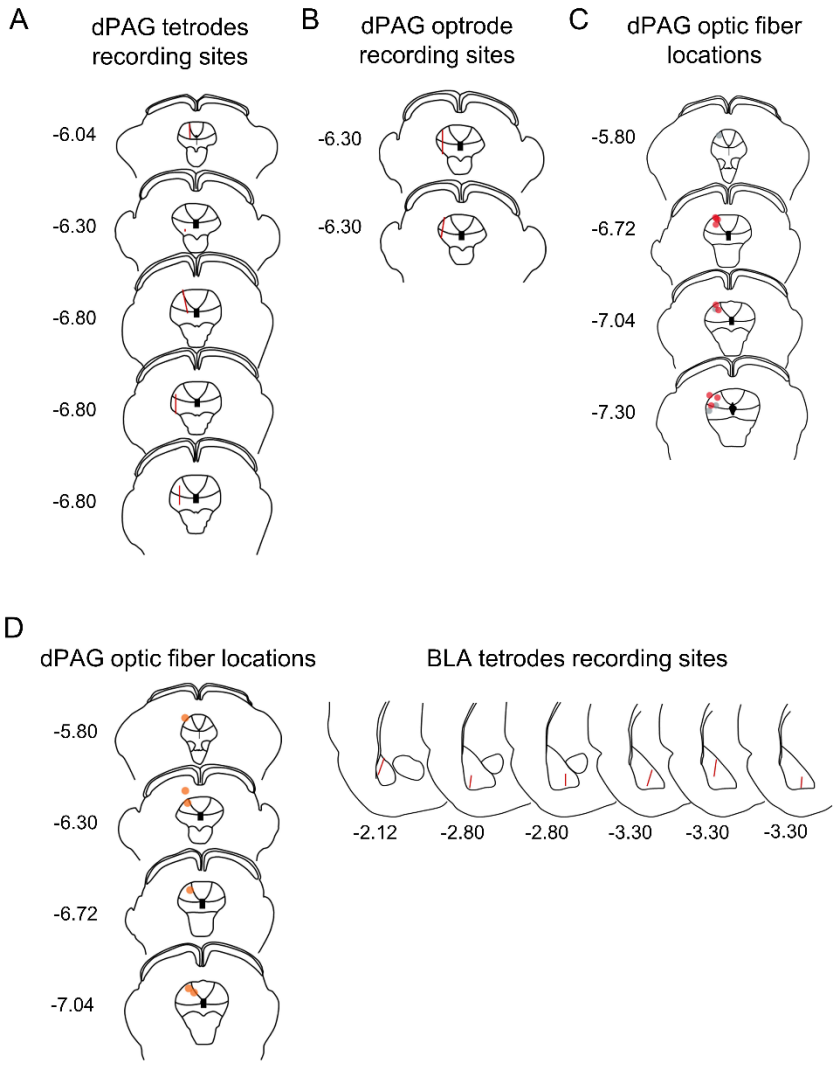

Figure S5. Histological reconstructions of the recording sites in the dPAG and BLA, and optic fiber locations in the dPAG. (A) Red bars indicate the trajectory of the tetrode recording sites in the dPAG. (B) Red bars indicate the trajectory of the optrode recording sites in the dPAG. (B) Red and gray circles indicate the optic fiber locations of the ChR2 and EYFP rats, respectively. (D) Orange circles and red bars indicate the optic fiber locations in the dPAG (*left*) and recording trajectories in the BLA (*right*). The numerical values represent AP coordinates relative to the Bregma.